THE ASTROPHYSICAL JOURNAL, 551:37–47, 2001 April 10


# A SEARCH FOR THE DAMPED Lyα ABSORBER AT $z = 1.86$ TOWARD QSO 1244+3443 WITH NICMOS

VARSHA P. KULKARNI,[1] JOHN M. HILL, AND GLENN SCHNEIDER
University of Arizona, Steward Observatory, Tucson, AZ 85721
RAY J. WEYMANN AND LISA J. STORRIE-LOMBARDI[2]
Carnegie Observatories, Pasadena, CA 91101
MARCIA J. RIEKE AND RODGER I. THOMPSON
University of Arizona, Steward Observatory, Tucson, AZ 85721
AND
BUELL T. JANNUZI
National Optical Astronomy Observatories, P.O. Box 26732, Tucson, AZ 85726-6732
*Received 2000 September 7; accepted 2000 December 12*

## ABSTRACT

We have carried out a high-resolution imaging search for the galaxy associated with the damped Lyα absorber (DLA) at $z = 1.859$ toward the $z_{em} = 2.48$ quasar QSO 1244+3443, using the *Hubble Space Telescope* (*HST*) and the near-infrared camera and multiobject spectrometer (NICMOS). Images were obtained in the broad filter F160W and the narrow filter F187N with camera 2 on NICMOS with the goal of detecting the rest-frame optical continuum and the Hα line emission from the DLA. After point-spread function (PSF) subtraction, two weak features are seen at projected separations of 0.″16–0.″24 from the quasar. Parts of these features may be associated with the DLA, although we cannot completely rule out that they could be artifacts of the PSF. If associated with the DLA, the objects would be $\approx 1$–$2\ h_{70}^{-1}$ kpc in size with integrated flux densities of 2.5 and 3.3 μJy in the F160W filter, implying luminosities at $\lambda_{central} = 5600$ Å in the DLA rest frame of $4.4$–$5.9 \times 10^9\ h_{70}^{-2}\ L_\odot$ at $z = 1.86$, for $q_0 = 0.5$. However, no significant Hα line emission is seen from these objects, suggesting low star formation rates (SFRs). Our 3 σ upper limit on the SFR in the DLA is $1.3\ h_{70}^{-2}\ M_\odot\ \mathrm{yr}^{-1}$ for $q_0 = 0.5$ ($2.4\ h_{70}^{-2}\ M_\odot\ \mathrm{yr}^{-1}$ for $q_0 = 0.1$). This together with our earlier result for LBQS 1210 + 1731 mark a significant improvement over previous constraints on the star formation rates of DLAs. Dust within the DLA could extinguish Hα emission, but this would require the dust content in the DLA to be much higher than that inferred from previous DLA observations. A combination of low star formation rate and some dust extinction is likely to be responsible for the lack of Hα emission. Alternatively, the objects, if real, may be associated with the host galaxy of the quasar rather than with the DLA. In any case, our observations suggest that the DLA is not a large bright protodisk, but a compact object or a low surface brightness galaxy. If the two features are PSF artifacts or associated with the quasar host, then the constraints on the size and luminosity of the DLA are even more severe.

*Subject headings:* cosmology: observations — galaxies: evolution — galaxies: high-redshift — infrared: galaxies — intergalactic medium — quasars: absorption lines

## 1. INTRODUCTION

Damped Lyα absorption (DLA) systems in quasar spectra contribute significantly to the neutral hydrogen content of the universe and are thought to be the progenitors of present-day galaxies. However, the exact nature of DLAs is not yet understood. DLAs are variously thought to be protospirals (Wolfe et al. 1986; Prochaska & Wolfe 1997, 1998), gas-rich dwarf galaxies (York et al. 1986; Matteucci et al. 1997), merging protogalactic fragments in cold dark matter cosmologies (e.g., Haehnelt et al. 1998), collapsing halos with merging clouds (e.g., McDonald & Miralda-Escudé 1999), or low surface brightness galaxies (Jimenez, Bowen, & Matteucci 1999). It has not been possible to determine which of these scenarios hold(s) true, because of the difficulty in detecting the emission from high-redshift DLAs.

Most attempts to detect the Lyα emission from high-redshift intervening ($z_{abs} < z_{em}$) DLAs have produced either nondetections or weak detections (e.g. Smith et al. 1989; Hunstead, Pettini, & Fletcher 1990; Lowenthal et al. 1995; Djorgovski et al. 1996; Djorgovski 1997). However these data do not effectively constrain the star formation rates (SFRs) in the DLAs, since even small quantities of dust can extinguish the Lyα emission, owing to the resonant scattering of the Lyα photons (Charlot & Fall 1991). Small but significant amounts of dust are indeed inferred to exist in DLAs from observations of reddening of background quasars and heavy-element depletion (e.g., Pei, Fall, & Bechtold 1991; Pettini et al. 1997; Kulkarni, Fall, & Truran 1997). There have been attempts to detect DLAs in longer wavelengths such as Hα, which are less affected by dust and not subject to resonant scattering. However, these either have resulted in nondetections or have only detected companions separated by large angular distances from the quasars (see, e.g, Teplitz, Malkan, & McLean 1998; Bechtold et al. 1998; Mannucci et al. 1998; Bunker et al. 1999). The detection of Hα emitters close to the quasar sight line has not been possible in high-$z$ intervening DLA

[1] University of South Carolina, Department of Physics and Astronomy, Columbia, SC 29208.
[2] SIRTF Science Center, California Institute of Technology, Pasadena, CA 91125.

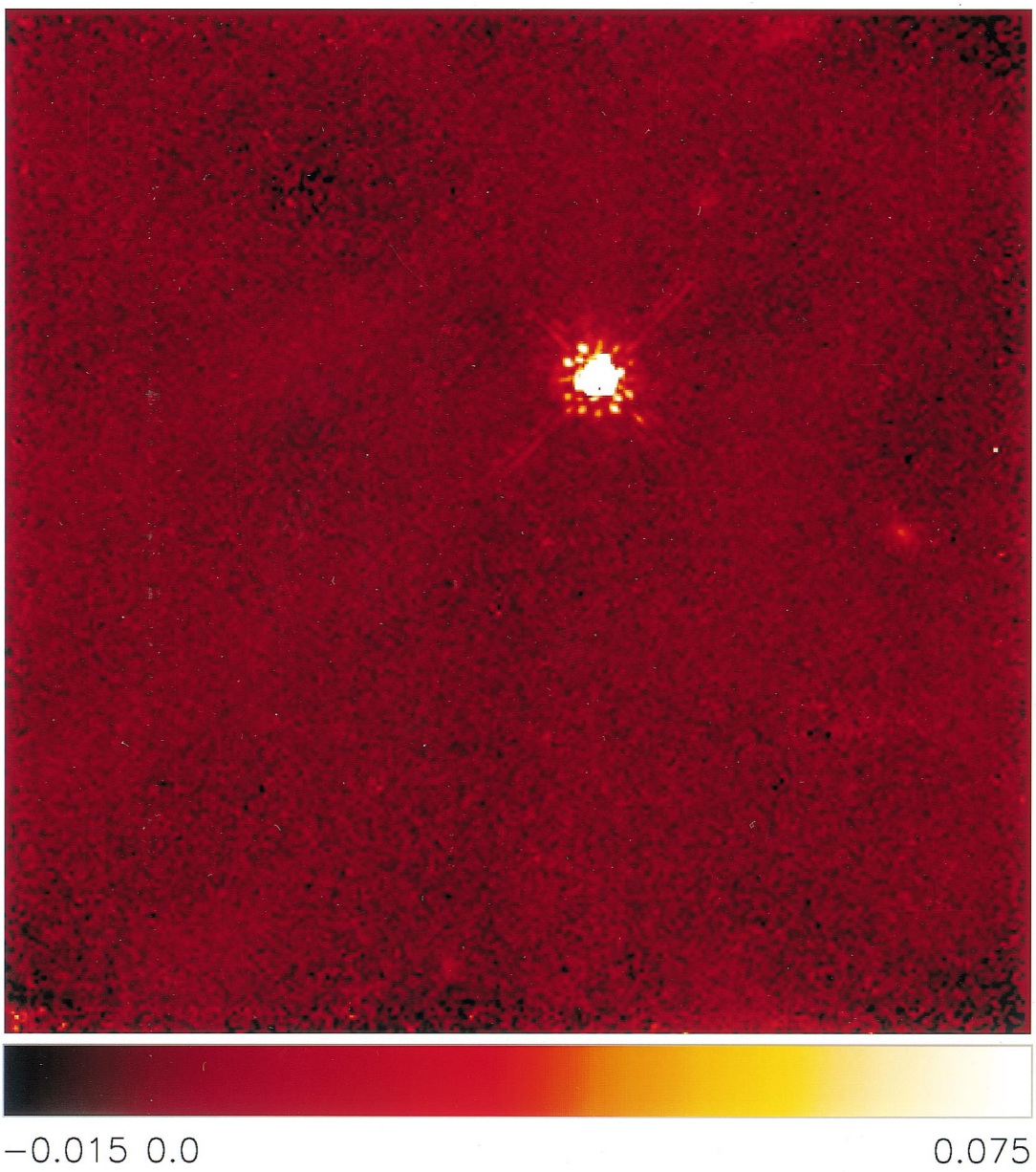


FIG. 1.—NICMOS camera 2 noncoronagraphic 1.6 $\mu$m broadband image of the field of QSO 1244 + 3443. The color scheme is indicated with the bar on the bottom of the image. Image $y$-axis is $-136\overset{\circ}{.}943$ east of north.

fields. A summary of the previous attempts to detect high-$z$ DLAs in emission is given by Kulkarni et al. (2000).

With the goal of searching for H$\alpha$-emitting objects at close separations from the quasar, we have obtained deep diffraction-limited images of three DLAs at $z \sim 2$ using the near-infrared camera and multiobject spectrometer (NICMOS) on board the *Hubble Space Telescope* (*HST*). In an earlier paper, we described the observations of the $z = 1.89$ DLA toward LBQS 1210+1731 in detail (Kulkarni et al. 2000). Here we describe our observations of the quasar 1244 + 3443 ($z_{\rm em} = 2.48$), which has a spectroscopically known damped Ly$\alpha$ absorber ($z_{\rm abs} = 1.859$ and log $N_{\rm HI} = 20.6$; Wolfe et al. 1995). Our observations combine high near-IR sensitivity and high spatial resolution with a more stable PSF than is currently possible with ground-based observations. Some of our observations also use the NICMOS coronagraph, which greatly decreases the scattered light background outside of the coronagraphic hole. Sections 2, 3, and 4 describe the observations, data reduction, and the subtraction of the quasar point spread functions. Our results are described in § 5. Finally, §§ 6 and 7 summarize the constraints from our observations on sizes, environment, and SFRs of DLAs.

## 2. OBSERVATIONS

The field of QSO 1244 + 3443 was observed at two epochs (1998 August 2 04:31–12:29 UT and 1998 July 5 18:32–21:22 UT), using NICMOS camera 2 (image scale $\sim 0\overset{''}{.}07598 \times 0\overset{''}{.}07530$, field of view $19\overset{''}{.}53 \times 19\overset{''}{.}3$). A sequence of spatially offset broadband images was obtained in MULTIACCUM mode with the F160W ($H$) filter (central wavelength 1.5940 $\mu$m, FWHM 0.4030 $\mu$m). Field offsetting was accomplished with a four-point spiral dither pattern in steps of $\approx 7.5$ pixels, using the field offset mirror (FOM) internal to NICMOS. The exposures at each dwell point were 640 s long, giving a total integration time of

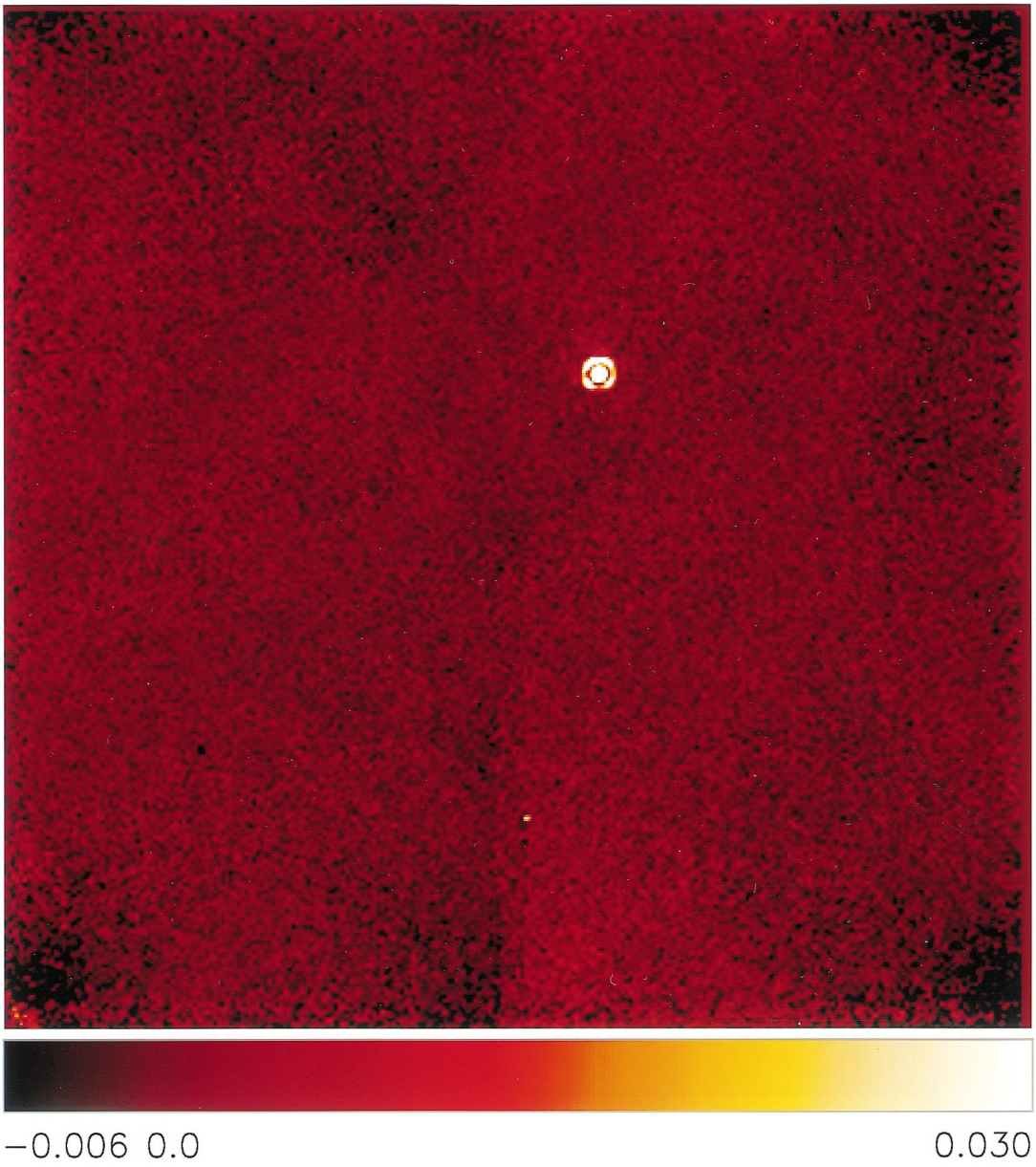


FIG. 2.—NICMOS camera 2 noncoronagraphic 1.9 $\mu$m narrowband image of the field of QSO 1244 + 3443. Image y-axis is −136°943 east of north.

2560 s. The MULTIACCUM observations consisted of nondestructive readouts in the "STEP64" readout timing sequence, i.e., "MULTIACCUM" readouts separated logarithmically up to 64 s and linearly in steps of 64 s beyond that. In addition, narrowband images were obtained in the filter F187N (central wavelength 1.875 $\mu$m, FWHM 0.0188 $\mu$m), in which the redshifted H$\alpha$ emission from the DLA, if present, would lie. Four-point spiral dither patterns in steps of 7.5 pixels, with a 704 s STEP64 MULTIACCUM exposure at each dwell point, were repeated in four successive orbits, resulting in a total integration time of 11,264 s. The spatial resolution of the F160W and F187N images is 0.″14 (1.8 pixels) and 0.″17 (2.1 pixels) FWHM, respectively. Thus, critical sampling is achieved with both filters by combining the dithered images onto a nearly optimal (half-pixel subsampled) grid.

Broadband images in the F160W filter were also obtained using the camera 2 coronagraph on 1998 July 5 from 18:32 to 21:22 UT. These consisted of an initial pair of 160 s long target acquisition images, which were followed by placement of the quasar in the coronagraphic hole (0.″3 or 4 pixels in geometrical radius) and then integration for a total of 5184 s (three exposures of 768 s each in the first orbit and three exposures of 960 s each in the second orbit, all using the STEP64 MULTIACCUM timing sequence). No dithering was used, of course, for the coronagraphic observations. The coronagraphic system significantly reduces both scattered and diffracted energy from the occulted target's point spread function core by factors of 4–6 in the region of $0.''55 < r < 1.''5$, compared to direct imaging (Schneider et al. 1998; Lowrance et al. 1998).

To circumvent image artifacts known as "bars" in all our camera 2 images, cameras 1 and 3 were run in parallel.

## 3. REDUCTION OF IMAGES

The images were reduced using the IRAF package NICRED 1.8 for the reduction of MULTIACCUM NICMOS data (McLeod 1997). The dark images used were

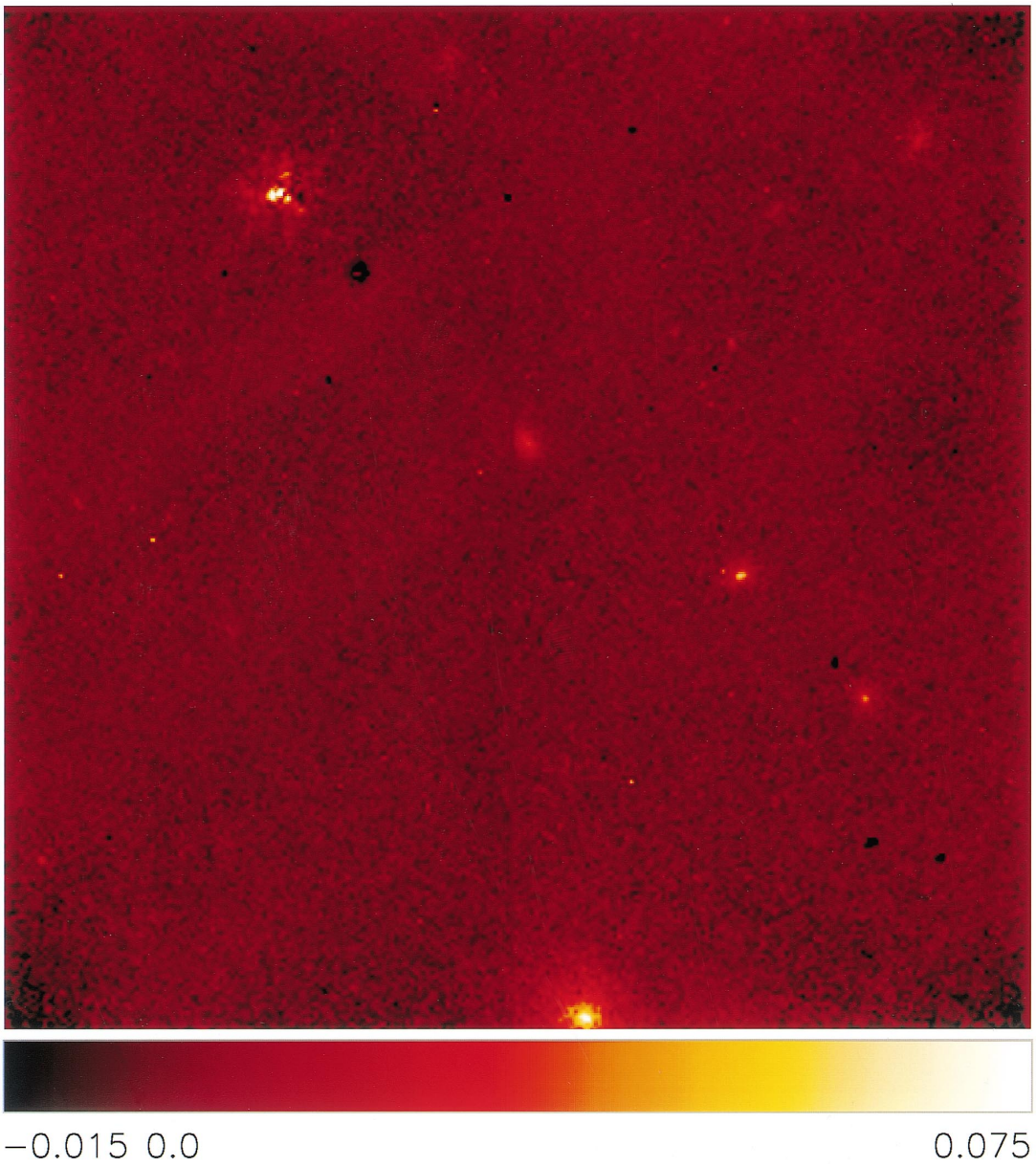


FIG. 3.—NICMOS camera 2 coronagraphic 1.6 $\mu$m broadband image of the field of QSO 1244 + 3443. The quasar has been placed in the coronagraphic hole. Image $y$-axis is $-117\overset{\circ}{.}897$ east of north.

made from on-orbit dark exposures taken during the NICMOS calibration program. For the noncoronagraphic images, the flat-field image used was made from on-orbit exposures taken with the internal calibration lamps during the NICMOS cycle 7 calibration program. For the coronagraphic images, the flat-field image was made with target acquisition data taken just before the coronagraphic exposures. This flat is far better, for regions close to the edge of the coronagraphic hole (and even out to $\approx 1''$), than the standard reference flats, which are severely affected by hole-edge gradients due to the relative motion of the hole. Use of the flat made with the target acquisition data ensures that the coronagraphic hole is in the same position on the detector as the quasar data, which is critical for studying faint objects close to the edge of the coronagraphic hole. See Kulkarni et al. (2000) for further details on the sequence of data reduction tasks performed by NICRED 1.8.

The images for the different dither positions were registered by cross-correlating with the IRAF task XREGISTER. The quasar was used as the reference object since it was the only point source available in our images. Finally, the registered images were averaged together using a bad pixel mask that took out any remaining bad pixels, and rejecting pixels deviating by more than 3 $\sigma$ from the average of the five F160W images, using averaged sigma clipping.

For the F187N images, where there were four exposures (one in each orbit) at each of the four dither positions, we first combined the four exposures at each position separately, and then registered and averaged the four positions together to make the final image. For the coronagraphic F160W images, where there were four exposures at the same position in each of the two orbits, we averaged the exposures in each orbit separately and then took a weighted average (weighting by exposure times) of the combined exposures from the two orbits.

Figures 1, 2, and 3 show the final reduced images for the

noncoronagraphic F160W, noncoronagraphic F187N, and coronagraphic F160W observations. The orientations of Figures 1 and 2 agree exactly while they differ from that of Figure 3 by 19°.046. The color table and the intensity scale in ADU $s^{-1}$ are shown below each figure. Figures 1 and 2 show the quasar point source along with the diffraction pattern. The quasar light has been reduced greatly (although not completely) in the coronagraphic image in Figure 3. A number of field galaxies are seen in the coronagraphic image at large angular separations from the quasar. To study whether there is any galaxy close to the quasar that may cause the DLA, we need to subtract the respective PSFs.

## 4. SUBTRACTION OF THE QUASAR POINT-SPREAD FUNCTION

To obtain reference point spread functions for subtraction, we used observations of stars in the same filter/aperture combinations as those employed for the quasar imaging. We did not include PSF star observations in our own observations since we wanted to maximize the use of the available *HST* observing time for imaging of the quasar fields. We therefore used PSF star observations from other programs (in particular the stellar images from the photometric monitoring program carried out during cycle 7 NICMOS calibration) for constructing the reference PSFs for subtraction.

For the noncoronagraphic images, we chose the PSF observations such that the telescope focus "breathing" (Bely 1993) values matched as closely as possible the values for the DLA observations. This attempts to minimize changes in the fine structure of the PSF caused by changes in the *HST* focus. For the noncoronagraphic F160W and F187N images, we used the PSF star P330E, observed on 1998 July 8 and 1997 August 5, respectively. The F160W noncoronagraphic image of P330E, made by combining four exposures of 3 s each, had a count rate of 108.10 ADU $s^{-1}$ at the maximum of the first Airy ring. The corresponding quasar image, made by combining four exposures of 640 s each, had a count rate of 0.99 ADU $s^{-1}$ at the maximum of the first Airy ring. For the F187N filter, the P330E image, made by combining three exposures of 80 s each, had 3.76 ADU $s^{-1}$ at the maximum of the first Airy ring. The corresponding count rate was 0.037 ADU $s^{-1}$ for the F187N quasar image, made by combining 16 exposures of 704 s each. See Kulkarni et al. (2000) for details on the selection of PSF stars with appropriate breathing values and for an in-depth discussion of the effect of breathing, color of PSF star, and other PSF details on the results of PSF subtraction.

For the coronagraphic observations, the PSF star was chosen such that the position of the star in the coronagraphic hole be as close as possible to that of the quasar in our observations. This is important, because the PSF wings and "glints" from the edge of the coronagraphic hole depend sensitively on the precise position of the point source within the hole. We therefore used the observations of star GL 577 for which we had coronagraphic observations (from another NICMOS GTO program), with the star placed at a position within 0.5 pixels of the position of the quasar QSO 1244 + 3443 in our data. (This was the closest available observed coronagraphic PSF to our quasar observations. Unfortunately, PSF stars with better matching locations in the hole were not available.) The observations of GL577 were taken on 1998 June 3 at a breathing value close to that for our quasar coronagraphic observations.

The PSF star observations were analyzed in exactly the same manner as the quasar observations. The same interpolation scheme was used for resampling of the PSF star and quasar images. (We note that differences in the sampling of the quasar and PSF star images could potentially give rise to some artifacts. However, the overall conclusions of our study are unaffected by whether or not the quasar and PSF images are resampled. See Kulkarni et al. 2000 for further details.) The reduced PSF star images were subtracted from the corresponding quasar images after suitable scaling and registration, using the IDL program "IDP-3" (Lytle et al. 1999). The relative $x$- and $y$-alignment of the PSF star image with respect to the quasar image and the intensity scaling factor for the PSF star image were fine tuned iteratively to obtain the minimum variance in roughly $3'' \times 3''$ subregions around the quasar in the PSF-subtracted image. Radial flux plots of the quasar image, the aligned and scaled PSF image, and the difference of the two were also examined to check the alignment and scaling of the PSF. Figures 4*a*, 5*a*, 6*a* show zoomed $\approx 2''.8 \times 2''.8$ subregions around the quasar, from the noncoronagraphic F160W, noncoronagraphic F187N, and coronagraphic F160W images shown in Figures 1, 2, and 3, respectively. Figures 4*b*, 5*b*, and 6*b* show the PSF-subtracted versions of Figures 4*a*, 5*a*, and 6*a*, respectively, using the closest matching PSFs available.

## 5. RESULTS

### 5.1. *Noncoronagraphic F160W Images*

Fig. 4*b* shows the F160W image after subtraction of the PSF image of star P330E dated 1998 July 8. The diffraction pattern disappears completely and most of the residual image contains a random mixture of positive and negative values. Two weak residuals are seen to remain near the quasar: One of the features is "below" the center, about 2 pixels (0".16) away from the center, while the second feature is to the "lower right" of the quasar, at a separation of about 0".24 from the quasar center. We name these features O1 and O2, respectively. (These features are seen more clearly if the data are subsampled by a factor of 2.) These features can not be made to disappear after reregistration of the PSF and quasar images or rescaling of the PSF image without causing large negative residuals elsewhere. We cannot completely rule out that O1 and O2 are artifacts in the PSF. However, given the significant excess over a number of pixels, it is likely that they are real. A detailed discussion of the effects of *HST* breathing and a number of other factors on the results of PSF subtraction in the field of quasar LBQS 1210+1731 is given in § 6 of Kulkarni et al. (2000).

Object O1 is $\approx 0''.2$ long, while object O2 is $\approx 0''.15$ long (just barely resolved) and more diffuse than O1. If O1 and O2 are associated with the DLA at $z = 1.859$, then they are $\approx 1.2$ and $0.9\ h_{70}^{-1}$ kpc long, respectively, for $q_0 = 0.5$, or 1.6 and $1.2\ h_{70}^{-1}$ kpc long for $q_0 = 0.1$. No other big, bright galaxies are seen near the quasar. We thus believe that the DLA absorber is either compact (e.g., a dwarf galaxy) or a low surface brightness galaxy.

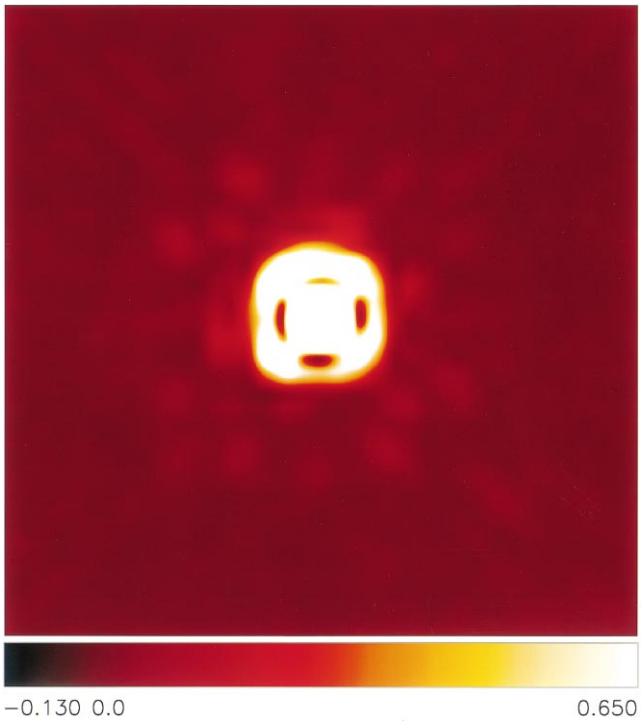


FIG. 4*a*

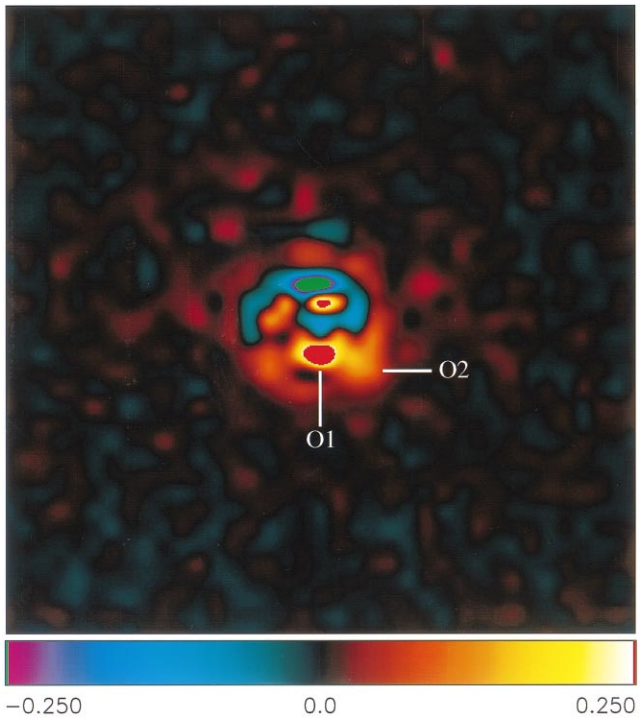


FIG. 4*b*

FIG. 4.—Zoomed-in 2″.81 × 2″.79 region of the NICMOS camera 2 noncoronagraphic 1.6 $\mu$m broadband image of the field of QSO 1244 + 3443, (*a*) before PSF subtraction, (*b*) after PSF subtraction.

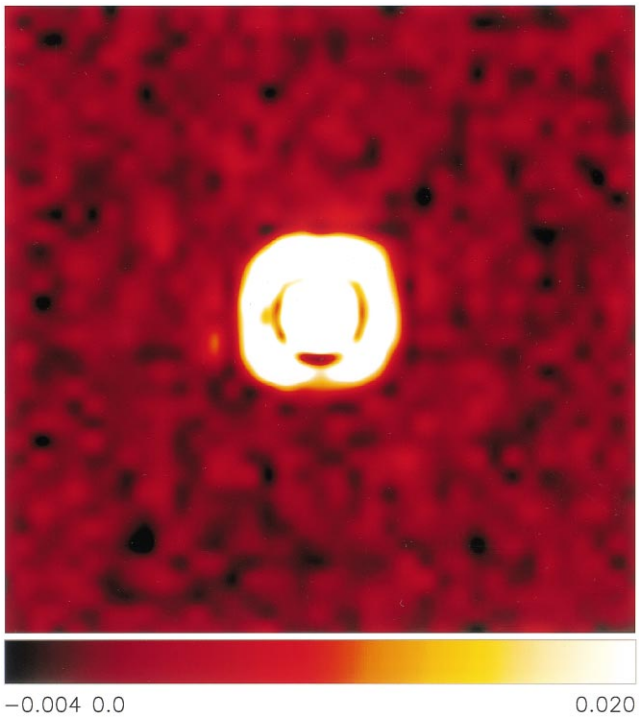


FIG. 5*a*

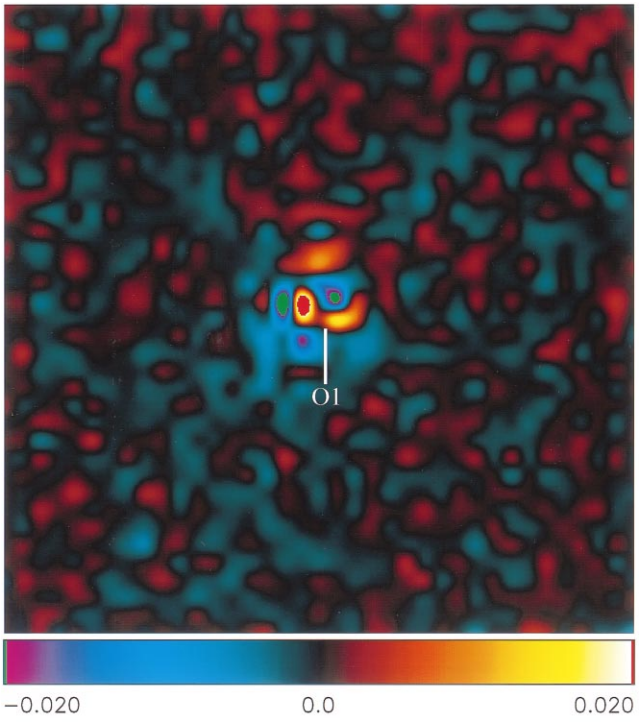


FIG. 5*b*

FIG. 5.—Zoomed-in 2″.81 × 2″.79 region of the NICMOS camera 2 noncoronagraphic 1.9 $\mu$m narrowband image of the field of QSO 1244 + 3443, (*a*) before PSF subtraction, (*b*) after PSF subtraction.

The photometry of O1 and O2 is difficult because of their faintness and diffuse nature. We estimated the fluxes by subtracting the PSF star from objects O1 and O2, now multiplying the star by factors large enough to make objects O1 and O2 look indistinguishable from noise. These PSF multiplying factors can then be used directly to estimate the fluxes of O1 and O2, since the PSF star P330E is also a well-calibrated NICMOS photometric standard. This implies a flux of 1.00 ADU $s^{-1}$ or 2.19 $\mu$Jy in the F160W filter, before aperture correction. To convert the count rate to flux, we used the NICMOS photometric calibration factor of $2.190 \times 10^{-6}$ Jy/(ADU $s^{-1}$) for the F160W filter,

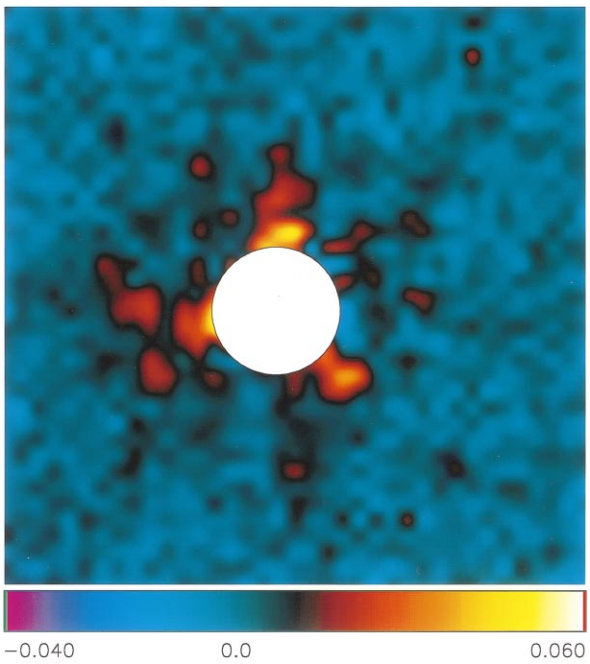


FIG. 6*a*

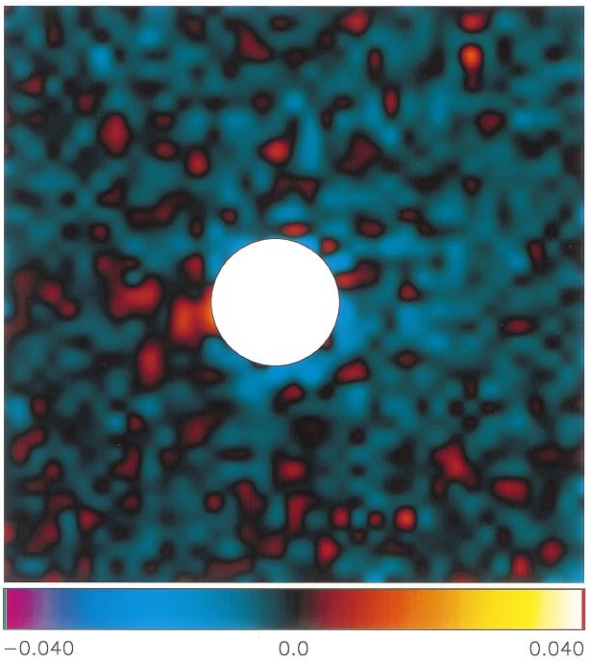


FIG. 6*b*

FIG. 6.—Zoomed-in 2″.81 × 2″.79 region of the NICMOS camera 2 coronagraphic 1.6 μm broadband image of the field of QSO 1244 + 3443, (*a*) before PSF subtraction, (*b*) after PSF subtraction.

derived using the solar-type photometric standard star P330E. For object O2, we similarly deduce a flux of 2.85 μJy in the F160W filter before aperture correction.

Since we had used an aperture of 7.5 pixels to do photometry of P330E, we corrected the above flux values of O1 and O2 slightly. The aperture correction factor from the flux within a 7.5 pixel radius aperture to the total flux has been estimated to be 1.152 for camera 2 filter F160W, based on standard NICMOS photometric calibrations made with P330E. Using this, we estimate fluxes of 2.52 μJy for O1 and 3.29 μJy for O2. For reference, the 1 σ noise level in the PSF-subtracted image is about 0.056 μJy pixel$^{-1}$ in a circular annulus 0″.2 wide centered at 0″.3 from the quasar center. The corresponding noise levels at 0″.5, 0″.7, 0″.9, and 1″.1 from the quasar center are 0.011, 0.0074, 0.0070, and 0.0066 μJy pixel$^{-1}$, respectively. Thus the formal 1 σ noise uncertainty in the total summed F160W flux over the regions occupied by O1 and O2 is ≈0.11 μJy (using the noise estimates just outside O1 and O2 at $r = 0''.3$). The errors in the flux values are likely to be larger than this estimate since O1 and O2 are barely resolved and are even closer to the quasar center.

The estimated fluxes of 2.52 and 3.29 μJy correspond to $m_{\rm F160W} = 21.58$ and 21.30, respectively, for O1 and O2, taking the zero magnitude to correspond to 1083 Jy in the Johnson system. These observed F160W fluxes correspond to luminosities (at mean rest frame wavelength of 5600 Å) of $4.4 \times 10^9\ h_{70}^{-2}\ L_\odot$ and $5.9 \times 10^9\ h_{70}^{-2}\ L_\odot$, respectively, for O1 and O2, for $q_0 = 0.5$. For $q_0 = 0.1$, these correspond to $8.2 \times 10^9\ h_{70}^{-2}\ L_\odot$ and $1.1 \times 10^{10}\ h_{70}^{-2}\ L_\odot$, respectively. Thus, objects O1 and O2 are fainter than an $L_*$ galaxy at $z = 1.86$ by 1.9–2.2 mag and 1.2–1.5 mag, for $q_0 = 0.5$ and $q_0 = 0.1$, respectively. If O1 and O2 are not the DLA, the DLA must be even fainter.

### 5.2. *Noncoronagraphic F187N Images*

At a redshift of $z_{\rm DLA} = 1.859$, any Hα emission would be expected to lie at $\lambda_{\rm obs} = 1.876$ μm, which is very close to the center wavelength λ of 1.874 μm for the filter F187N. Thus, the narrowband images in filter F187N are expected to reveal any redshifted Hα emission from the DLA. Figure 5*b* shows the PSF-subtracted F187N image using the PSF image of the star P330E observed on 1997 August 5. The residual image shows a noisy feature in roughly the same place and with roughly the same size as the feature O1 seen in the noncoronagraphic F160W image. But this feature is very weak and could be a PSF artifact. No corresponding feature is seen for object O2.

As in the case of the broadband images, the photometry of O1 is rather difficult. Subtracting the standard star P330E from O1, scaling the star such that O1 just disappears, we estimate a flux of 2.62 μJy for O1. Here we have used the NICMOS photometric calibration factor of $4.107 \times 10^{-5}$ Jy/(ADU s$^{-1}$) for the F187N filter. For comparison, the 1 σ noise levels in the F187N image (after PSF subtraction) at $r = 0''.5$, 0″.7, 0″.9, and 1″.1 from the quasar are 0.033, 0.033, 0.031, and 0.030 μJy pixel$^{-1}$, respectively. Thus the formal 1 σ sky noise uncertainty in the total summed F187N flux over the region occupied by O1 and O2 is ≈0.13 μJy (using the noise estimates just outside O1 and O2 at $r = 0''.3$). Again, the uncertainty in the fluxes is likely to be greater than this estimate because O1 is very faint, almost unresolved, and even closer to the quasar center.

The expected F187N continuum must be subtracted from the observed flux in order to determine if a statistically significant redshifted Hα excess exists. We estimate the continuum under the F187N filter by scaling the F160W image using the relative photometric calibration of the two filters. We find that, in fact, this expected continuum flux agrees almost completely with the observed F187N flux. The 1 σ noise level in the F187N−F160W image is 0.018 μJy pixel$^{-1}$ just outside the location of O1 and O2. This noise level corresponds to a 1 σ uncertainty of 0.074 μJy in the total flux summed over the region occupied by O1. We therefore conclude that the contribution to the F187N flux from redshifted Hα emission is negligible even for O1. It is not likely that we could have missed the Hα emission from O1. The Hα emission from the DLA could lie outside the

F187N bandpass only if the DLA galaxy is lower in velocity by more than 1730 km $s^{-1}$ or higher in velocity by more than 1280 km $s^{-1}$ from the absorption redshift. Such offsets are higher than the observed internal velocity dispersion in any typical single galaxy.

In a $2 \times 2$ pixel region (roughly the size of our resolution element), an H$\alpha$ emission strength of about 0.223 $\mu$Jy would yield signal-to-noise ratio (S/N) = 3. With an aperture correction factor of 3.37, this corresponds to a total 3 $\sigma$ flux limit of 0.75 $\mu$Jy. Integrating over the FWHM of the F187N filter, assuming no dust extinction, and using the prescription of Kennicutt (1983) for conversion of H$\alpha$ luminosity to SFR, we get a 3 $\sigma$ upper limit on the SFR of 1.3 $h_{0.7}^{-2}$ $M_\odot$ $yr^{-1}$ for $q_0 = 0.5$ or 2.4 $h_{0.7}^{-2}$ $M_\odot$ $yr^{-1}$ for $q_0 = 0.1$.

Thus we conclude that the broadband images suggest possible detections of objects O1 and O2 at 0".16 and 0".24 from the quasar center, although no significant H$\alpha$ emission is detected from either of them. We cannot completely rule out that these features could be artifacts of the PSF. In that case, our images put very sensitive upper limits on the size and brightness of both the DLA absorber and the quasar host. We discuss these constraints in § 6.

### 5.3. *Coronagraphic F160W Images*

An F160W coronagraphic image of the central $\sim 3''$ region near the quasar is shown in Figure 6*a*, in which the coronagraphic hole is masked out. Almost all the flux seen in this reduced coronagraphic image is due to residual scattered light from the quasar and "glints" from the edge of the hole. After subtraction of a reference PSF image using observations of the star GL 577, these artifacts disappear almost entirely (Fig. 6*b*). Features O1 and O2 seen in Figures 4*b* and 5*b* are just inside the coronagraphic hole and are therefore not seen in Figure 6*b*. However, the coronagraph is very effective in reducing the quasar light outside of the coronagraphic hole and can therefore be used to look at other objects in the field.

The bright glint immediately to the lower left of the edge of the coronagraphic hole is unlikely to be real. This is because this particular positive "glint" has been seen in many other PSF subtractions taken at slightly different subtractions of other targets where the breathing phase differential is slightly negative in target-PSF subtractions. Furthermore, as noted above, there is a mismatch of about 0.5 pixel between the positions of the PSF star and the quasar inside the coronagraphic hole. Unfortunately, a better matching PSF star was not available. In any case, no other significant objects are seen close to the quasar. A number of galaxies are seen farther from the quasar in the coronagraphic image (Fig. 3). We will discuss these further in § 6.1 below.

## 6. DISCUSSION

The most important result from our observations is that no large bright galaxies are seen close to the quasar in the field of the DLA absorber toward QSO 1244+3443. Features O1 and O2 are the only detected candidates within several arcseconds of the quasar and, if real, may be associated with the DLA. Their redshift is not confirmed since no H$\alpha$ emission is detected from them. In §§ 6.1 and 6.2, we assume that object O1 is associated with the DLA to derive constraints on various properties of DLAs. But we also consider alternative possibilities in § 6.3, mainly the possibility that O1 and O2 may be associated with the host galaxy of the quasar. If O1 and O2 are PSF artifacts, then the constraints on the DLA and the quasar host are even more severe.

### 6.1. *Constraints on Sizes, Morphology, and Environments of DLAs*

Our observations show no evidence for a big, well-formed galaxy as expected in some scenarios for the DLAs (e.g., the protospiral model suggested by Wolfe et al. 1986; Prochaska & Wolfe 1997, 1998; Jedamzik & Prochaska 1998). Features O1 and O2 have estimated sizes of 1–2 $h_{70}^{-1}$ kpc, if they are real and are at the redshift of the DLA. This suggests that the absorber is compact and clumpy, as expected in the hierarchical picture of DLAs. But it is possible that O1 and O2 are the brightest regions within a bigger galaxy, the rest of which we cannot see. Thus, we cannot completely rule out the large disk scenario, although the compact sizes and low SFRs suggest that the hierarchical picture may be favored. Further deeper observations will help to more definitively distinguish between the large disk versus hierarchical models.

Apart from features O1 and O2 very close to the quasar, our images show several galaxies in the F160W and F187N images. In particular, the coronagraphic F160W image shows seven galaxies, one of which is very bright while three are moderately bright galaxies aligned in almost a straight line with the quasar, roughly to the east of the quasar. The other three are fainter. The closest galaxy in roughly the east direction is also seen in the noncoronagraphic F160W image, and barely seen in the F187N image. The other galaxies seen in the coronagraphic F160W image are outside the field of the noncoronagraphic images and thus not seen in them. From the galaxy number count-magnitude relation based on deep NICMOS images (Yan et al. 1998), about one galaxy is expected for $H < 21$ in the camera 2 field. In comparison, the high density of galaxies in our NICMOS images suggests that several of these galaxies may belong to the same group as the DLA, and clustering may be enhanced near this DLA. (However, we do not have redshift information on these galaxies.) In any case, they have fairly large angular separations from the quasar (3".9, 6".7, 9".2, 11".3, 12".0, 14".6, and finally 16".8 for the bright galaxy), suggesting it is unlikely for any of them to be the DLA absorber itself.

### 6.2. *Contraints on Star Formation Rate and Dust in DLAs*

The lack of significant rest-frame H$\alpha$ emission in our images puts fairly tight constraints on the star formation rate in the DLA toward QSO 1244 + 3443, i.e., a 3 $\sigma$ upper limit of 1.3 (2.4) $h_{70}^{-2}$ $M_\odot$ $yr^{-1}$ for $q_0 = 0.5$ (0.1), if no dust is assumed. This is similar to (even smaller than) the upper limit on the SFR in the high-$z$ DLA toward LBQS 1210 + 1731 (Kulkarni et al. 2000), i.e., a 3 $\sigma$ constraint of 4 $h_{70}^{-2}$ $M_\odot$ $yr^{-1}$ for $q_0 = 0.5$ or 7.4 $h_{70}^{-2}$ $M_\odot$ $yr^{-1}$ for $q_0 = 0.1$. For comparison, the near-IR spectroscopic survey of Bunker et al. (1999), aimed at detecting H$\alpha$ from DLAs, gave typical upper limits of $\approx 15$ $M_\odot$ $yr^{-1}$, for $q_0 = 0.5$, and $H_0 = 70$ km $s^{-1}$ $Mpc^{-1}$. Our limits on the SFR in QSO 1244+3443 and LBQS 1210+1731 mark a big improvement over the tightest previous constraints on the SFR in DLA galaxies from H$\alpha$ spectroscopy (see Fig. 19 of Kulkarni et al. 2000 for a detailed comparison).

In principle, the lack of detectable H$\alpha$ emission from the DLA could be because of dust extinction, in which case the

actual SFR could be higher. However, if the H I column density weighted average SFR was that predicted by the closed box model of Pei & Fall (1995) and if DLAs are large disks, with the global SFR distributed among them, then to reconcile the prediction of 38.5 $M_\odot$ yr$^{-1}$ at $z = 1.86$ to a value below our upper limit, one would require an optical depth $\tau_{0.66\mu m} > 3.4$ (see Fig. 19 of Kulkarni et al. 2000 for the predictions of the closed-box model for large disks). This implies an optical depth at 4400 Å of $\tau_B > 5.8$ and hence a mean dust-to-gas ratio $k \equiv \tau_B(10^{21}/N_{\rm HI}) > 14.6$. Here we have assumed an extinction curve similar to that of the Milky Way or the Small Magellanic Cloud or the Large Magellanic Cloud. Dust-to-gas ratios $k > 14.6$ are much higher than the mean dust-to-gas ratio of 0.8 for the Milky Way, or the typical value of $\sim$ 0.03–0.1 for the DLA galaxies, suggested by observations of background quasar reddening and heavy-element depletions (see, e.g., Pei et al. 1991; Pettini et al. 1997 and references therein).

One could ask whether the DLA may be simply hiding because parts of it could be very dusty. This is a possibility since the regions of DLAs probed by spectroscopy of quasars may be systematically less dusty. Such a selection effect could arise because the dustier regions would extinguish the quasar (see, e.g., Fall & Pei 1993). However, as discussed above, it would take a dust-to-gas ratio of greater than 14.6 (and $A_{H-\alpha} > 3.7$ mag) to extinguish the Hα emission expected at the average SFR predicted for a large-disk DLA at $z = 1.86$. Thus if the regions of the DLA away from the quasar sight line were to have their Hα emission extinguished by dust, the dust-to-gas ratio would have to change by a factor of several hundred from the line of sight to the quasar to all off line directions. Such a situation is possible, but seems rather contrived. In this context, we note that Glazebrook et al. (1999) observed a sample of 13 Canada-France Redshift Survey galaxies at $z \sim 1$ in redshifted Hα. They found that the SFR from Hα is $\sim$3 times that inferred from the UV and that the extinction is moderate, with $A_V \sim 1$ at most for these galaxies. Kennicutt (1998) discusses the merits of and the systematic errors in using Hα to derive SFRs. He reports a mean extinction $A_{H-\alpha}$ of 0.5–1.8 mag for large samples of H II regions in nearby galaxies. Thus there is no reason to expect the $z = 2$ DLAs to have extinction much higher than these amounts. It seems more natural to interpret the lack of Hα in terms of a low star formation rate assuming reasonable numbers for the dust-to-gas ratio. The real picture may be a combination of low star formation rate and some (moderate) amount of dust extinction. If the SFR is indeed low, then this together with the compact sizes seen in our images suggests that the DLA may be a dwarf galaxy or a low surface brightness (LSB) galaxy, rather than a large bright disk.

To compare our relative sensitivity to detection of various kinds of galaxy morphologies, we have carried out simulations for disk and LSB galaxies. Using our observed noncoronagraphic F160W image of QSO 1244+3443, we created a simulated image by adding disks or LSBs of varying brightnesses at angular separations of 1.″0 from the quasar (taken as a representative angular separation of interest). The simulated images were made using the IRAF task MKOBJECTS and then PSF subtracted in a manner similar to that used for the actual quasar image. The magnitudes of the galaxies were varied to see how faint these objects have to be in order not to be detected in our F160W NICMOS image even after PSF subtraction. A disk with an exponential surface brightness profile and a scale length of 3 $h_{70}^{-1}$ kpc was placed at a separation of 1″ in projection from the quasar. Such a disk galaxy would be barely detectable in our observations if the disk had $H = 22$, and more easily detectable with $H < 21$. For a low surface brightness galaxy, we assume an exponential brightness profile with a scale length of 14 $h_{70}^{-1}$ kpc (i.e., 10 $h_{100}^{-1}$ kpc, the average scale length of a giant LSB galaxy—see Sprayberry et al. 1995). We find that such a giant LSB galaxy when placed 1″ away from the quasar would be hard to detect in our F160W image even after PSF subtraction, if it had an integrated H magnitude of $H \geq 19$. On the other hand LSBs with $H \leq 18.5$ would be detectable at separations of 1 ″ from the quasar (more easily so for $H \leq 18$).

We also note that an LSB galaxy with $H = 18$ separated 1″ away from the quasar would have been easy to detect and would in fact look roughly similar (in shape, size and brightness) to the halo left behind around the quasar after PSF subtraction in our actual observed image (Fig. 4*b*). Thus it would be hard to distinguish between the PSF subtraction residuals and an LSB of $H = 18$ positioned exactly on top of the quasar. However, since the circumquasar residuals seen in our F160W image correspond well in positions of detailed features with the features in the PSF of a star like P330E, we take the view that the faint halo seen around the quasar after PSF subtraction (Fig. 4*b*) is indeed because of PSF subtraction residuals rather than an LSB galaxy of $H = 18$. This and the fact that no $H \geq 19$ LSBs are detectable clearly underscore the possibility that our NICMOS F160W image could be hiding a large LSB at angular separations as close as (or closer than) 1″ from the quasar.

We expect that in comparison to LSBs, compact objects should be much easier to detect. At the close angular separations of features O1 and O2 from the quasar, we expect the detection of disks and LSBs to get harder than estimated in the above simulations. Features O1 and O2 have $H = 21.58$ and 21.30, respectively, somewhat brighter than the $H = 22$ limit of detection for a normal disk 1″ away, but much fainter than the detection limit of $H = 19$ for an LSB 1″ away. Thus, if these features are real, they may be compact, dwarf galaxies themselves or they could be parts of larger disks or LSBs. The lack of any other objects in regions farther out (at separations comparable to 1″ from the quasar) can rule out presence of disks with $H \leq 22$ or LSBs with $H \leq 19$. The limits are even tighter for separations out to 6.″7, which is the separation of the nearest galaxy detected in the observed noncoronagrahic F160W image, or even out to 3.″9, the separation of the nearest galaxy detected in the coronagraphic F160W image.

### 6.3. *Alternative Possibilities*

Finally, if O1 and O2 are real, it is possible that they arise in the quasar host galaxy, rather than the DLA. We cannot test this possibility further because we do not have narrow-band images in filters tuned to $z_{\rm em} = 2.48$. However, we cannot rule out this possibility either. If O1 and O2 are in fact associated with the host galaxy of the quasar, then they would have luminosities (at rest frame 0.46 $\mu$m) of $\approx 8.4 \times 10^9\ h_{70}^{-2}\ L_\odot$ and $1.1 \times 10^{10}\ h_{70}^{-2}\ L_\odot$, respectively, for $q_0 = 0.5$ ($1.8 \times 10^{10}\ h_{70}^{-2}\ L_\odot$ and $2.4 \times 10^{10}\ h_{70}^{-2}\ L_\odot$, respectively, for $q_0 = 0.1$). The images would then suggest that the quasar host is not a large galaxy with or without interactions, but rather shows a compact morphology. The

strongest feature in the quasar host would then be off-center with respect to the quasar nucleus, which has been observed in other quasars. If O1 and O2 are in fact the quasar host, then the limits on the luminosity and SFR in the DLA are even more severe than our estimates in §§ 5.1 and 5.2. Conversely, if the features are associated with the DLA galaxy, then the constraints on the quasar host are more severe than those given above.

It is also possible that we may be seeing interloper galaxies at redshifts other than that of the DLA. In this context, we note that ground-based spectra of QSO 1244+3443 have revealed three other absorbers besides the DLA, at $z = 1.8444$, 1.8491, and 1.9126 (Wolfe et al. 1993). These absorbers may explain some of the galaxies seen at larger angular separations from the quasar (Fig. 3). Indeed the absorbers at $z = 1.8444$ and 1.8491 may belong to the same group of galaxies as the DLA. Our narrowband searches, which failed to detect any line emission at all, would have been able to detect rest-frame Hα emission from even the absorbers at $z = 1.8444$ and 1.8491. We do not have Hα images at the redshift of the absorber at $z = 1.9126$. Thus we cannot test the interloper possibility further. However, since the other absorbers are not DLAs and have weaker Lyα and metal absorption lines than the DLA, they seem less likely to be detectable than the DLA itself.

### 6.4. *Comparison with Other Work*

Recently, Warren et al. (2000) have presented analysis of a NICMOS broadband imaging survey in the F160W filter for 15 quasars with DLAs. Their method of PSF subtraction is different from ours. For each quasar in their sample, they use the average of their other 14 observed quasar images to create a PSF for subtraction. This has the advantage of achieving a good color match (as compared to using a stellar PSF) and also having the PSF image land upon nearly the same subpixel locations as for the quasar. However it does reduce the possibility of detecting the quasar host galaxies or diffuse (e.g., low surface brightness) galaxies at very small angular separations from the quasar. We take the approach of using the observed PSFs of stars, taking care of pixel nonlinearization effects in data reduction with NICRED and subpixel positioning accuracy between quasar and PSF star in IDP-3. This allows us to be more sensitive to detecting quasar hosts or diffuse objects very close to the quasar. Warren et al. (2000) estimate that the accuracies of the two PSF subtraction techniques are comparable (probably more so at larger angular separations–above ≈0.″5–0.″6.) Indeed features O1 and O2 here and in LBQS 1210+1731 (Kulkarni et al. 2000) appear comparable to the object N12-1D of Warren et al. (2000). We believe that object could also be a DLA, either a compact object or the brightest part of a bigger galaxy; alternatively, it could also be the quasar host galaxy. Overall, our results are consistent with those of Warren et al. (2000), who also find no large bright galaxies in their NICMOS survey.

## 7. CONCLUSIONS AND FUTURE WORK

Our continuum and Hα images of the $z = 1.86$ DLA toward QSO 1244+3443 suggest that this DLA is not a big galaxy with high SFR, but may be compact (1–2 $h_{70}^{-1}$ kpc in size), probably consisting of multiple subunits. A few possibly companion galaxies are seen at larger angular separations in the continuum images. Assuming no dust extinction of Hα emission, we place a 3 $\sigma$ upper limit of 1.3 (2.4) $h_{70}^{-2}$ $M_\odot$ yr$^{-1}$ on the star formation rate, for $q_0 = 0.5$ (0.1). Our observations are consistent with the hierarchical models, in which DLAs arise in several subgalactic clumps or dwarf galaxies, which eventually come together to form the present-day galaxies (see, e.g., York et al. 1986; Matteucci et al. 1997). Indeed, theoretical simulations of merging protogalactic fragments in cold dark matter cosmologies (e.g., Haehnelt et al. 1998) and collapsing halos with merging clouds (e.g., McDonald & Miralda-Escudé 1999) have been found to reproduce the observed asymmetric line profiles in metal absorption lines of DLA galaxies. However, it cannot be ruled out that the DLA toward QSO 1244 + 3443 is a large low surface brightness galaxy with a low SFR, the rest of which is below our detection limit even in the F160W image.

Our results for QSO 1244 + 3443 agree with our earlier results for LBQS 1210+1731 and results for our remaining NICMOS observations (Kulkarni et al. 2000, 2001, in preparation). The findings of the NICMOS broadband imaging study by Warren et al. (2000) also agree with our broadband results here. In the end, to verify the reality of all our candidate objects and similarly those of Warren et al. (2000), confirming spectroscopy or narrowband imaging is necessary. The lack of significant Hα detections in our observations suggests that it will be very helpful to have deep Lyα imaging with STIS or deeper near-IR narrowband imaging with NICMOS when it becomes available again. Narrowband imaging observations will help to establish the redshift identifications of the DLAs, their companion galaxies, and quasar host galaxies, and are likely to be more efficient than spectroscopy. It is also necessary to increase the number of imaging studies of high-$z$ DLAs, since the current sample of DLAs studied at high resolution to search for Hα emission is still small. It is quite possible that different DLAs have different rates of evolution because of different physical conditions. Indeed, this is suggested by the large scatter in the metallicity-redshift relation of DLAs (see, e.g., Pettini et al. 1997, 1999 and references therein). To improve the statistics of the DLA imaging studies, it is necessary to obtain high spatial resolution near-IR images of more high-redshift DLAs. A major advantage of future *HST* observations will be relatively stable PSFs compared to those currently achieved with ground-based telescopes, a factor that is crucial for the detection of DLAs. It will also be of great interest to complement the *HST* observations with observations from adaptive optics systems on large ground-based telescopes. Although these systems do not currently have the relatively stable PSF offered by *HST*, they will be able to achieve even higher spatial resolution and higher imaging sensitivity. Such combined future space and ground-based observations will provide further insight into the structure and nature of DLAs and their relation to other galaxies.

This project was supported by NASA grant NAG 5-3042 to the NICMOS Instrument Definition Team. It is a pleasure to thank Nicholas Bernstein and Keith Noll for their assistance in the scheduling of our observations. We thank E. Stobie, D. Lytle, E. O'Neil, I. Barg, and A. Ferro for software and computer support.

REFERENCES

Bechtold, J., Elston, R., Yee, H. K. C., Ellingson, E., & Cutri, R. M. 1998, in ASP Conf. Ser. 146, The Young Universe: Galaxy Formation and Evolution at Intermediate and High Redshift, ed. S. D'Odorico, A. Fontana, & E. Giallongo (San Francisco: ASP), 241
Bely, P. 1993, STScI Rep. SESD-93-16 (Baltimore: STScI)
Bunker, A. J., Warren, S. J., Clements, D. L., Williger, G. M., & Hewett, P. C. 1999, MNRAS, 309, 875
Charlot, S., & Fall, S. M. 1991, ApJ, 378, 471
Djorgovski, S. G. 1997 in Proc. IAP Colloq. 13, Structure and Evolution of the IGM from the QSO Absorption Line Systems, ed. P. Petitjean & S. Charlot (Paris: Edition Frontières), 303
Djorgovski, S. G., Pahre, M. A., Bechtold, J., & Elston, R. 1996, Nature, 382, 234
Fall, S. M., & Pei, Y. C. 1993, ApJ, 402, 479
Glazebrook, K., Blake, C., Economou, F., Lilly, S., & Colless, M. 1999, MNRAS, 306, 843
Haehnelt, M., Steinmetz, M., Rauch, M. 1998, ApJ, 495, 647
Hunstead, R. W., Pettini, M., & Fletcher, A. B. 1990, ApJ, 356, 23
Jedamzik, K., & Prochaska, J. X. 1998, MNRAS, 296, 430
Jimenez, R., Bowen, D. V., & Matteucci, F. 1999, ApJ, 514, L83
Kennicutt, R. C. 1983, ApJ, 272, 54
———. 1998, ARA&A, 36, 189
Kulkarni, V. P., Fall, S. M., & Truran, J. W. 1997, ApJ, 484, L7
Kulkarni, V. P., Hill, J. M., Weymann, R. J., Storrie-Lombardi, L. J., Rieke, M. J., Schneider, G., Thompson, R. I., & Jannuzi, B. 2000, ApJ, 536, 36
Lowenthal, J. D., Hogan, C. J., Green, R. F., Woodgate, B. E., Caulet, A., Brown, L., & Bechtold, J. 1995, ApJ, 451, 484
Lowrance, P. et al. 1998, in Proc. NICMOS and the VLT, ed. W. Freudling & R. Hook (Garching: ESO), 96
Lytle, D., Stobie, E., Ferro, A., & Barg, I. 1999, ASP Conf. Ser. 172, Astronomical Analysis Software and Systems 8, ed. D. Mehringer, R. Plante, & D. Roberts (San Francisco: ASP), 445
Mannucci, F., Thompson, D., Beckwith, S. V. W., & Williger, G. M. 1998, ApJ, 501, L11
Matteucci, F., Molaro, P., & Vladilo, G. 1997, A&A, 321, 45
McDonald, P., & Miralda-Escudé, J. 1999, ApJ, 519, 486
McLeod, B. 1997, in Proc. 1997 *HST* Calibration Workshop, ed. S. Casertano et al. (Baltimore: STScI), 281
Pei, Y. C., & Fall, S. M. 1995, ApJ, 454, 69
Pei, Y. C., Fall, S. M., & Bechtold, J. 1991, ApJ, 378, 6
Pettini M., Ellison, S. L., Steidel, C. C., & Bowen, D. V. 1999, ApJ, 510, 576
Pettini, M., King, D. L., Smith, L. J., & Hunstead, R. W. 1997, ApJ, 478, 536
Prochaska, J. X., & Wolfe, A. M. 1997, ApJ, 487, 73
———. 1998, ApJ, 507, 113
Schneider, G., Thompson, R. I., Smith, B. A., & Terrile, R. J. 1998, Proc. SPIE, 3356, 222
Smith, H. E., Cohen, R. D., Burns, J. E., Moore, D. J., & Uchida, B. A. 1989, ApJ, 347, 87
Sprayberry, D., Impey, C. D., Bothun, G. D., & Irwin, M. J. 1995, AJ, 109, 558
Teplitz, H. I., Malkan, M., & McLean, I. S. 1998, ApJ, 506, 519
Warren, S. J., Møller, P., Fall, S. M., & Jakobsen, P. 2000, MNRAS, submitted
Wolfe, A. M., Lanzetta, K. M., Foltz, C. B., & Chaffee, F. H. 1995, ApJ, 454, 698
Wolfe, A. M., Turnshek, D. A., Lanzetta, K. M., & Lu, L. 1993, ApJ, 404, 480
Wolfe, A. M., Turnshek, D. A., Smith, L. J., & Cohen, R. D. 1986, ApJS, 61, 249
Yan, L., McCarthy, P. J., Storrie-Lombardi, L. J., & Weymann, R. J. 1998, ApJ, 503, L19
York, D. G., Dopita, M., Green, R., & Bechtold, J. 1986, ApJ, 311, 610